AD-A111 537 SOLAR TURBINES INTERNATIONAL SAN DIEGO CA F/6 11/6
EROSION MECHANISMS OF METALS.(U)
NOV 81 K G KUBARYCH, M E GULDEN F49620-78-C-0104
UNCLASSIFIED SR81-R-4526-02 AFOSR-TR-82-0080 NL

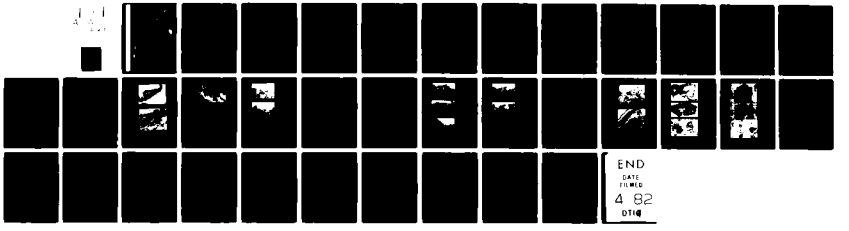

END
DATE FILMED
4 82
DTIC

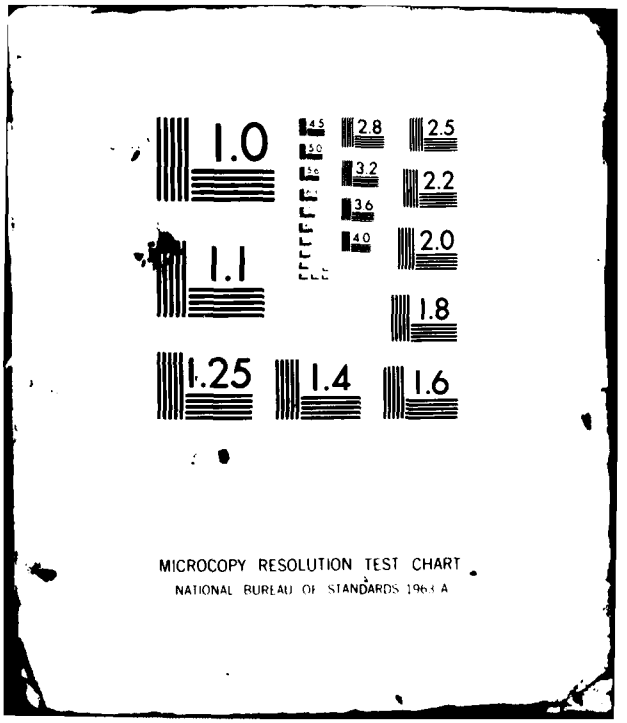
1.0
1.1
1.25
1.4
1.6
2.8
3.2
3.6
4.0
2.5
2.2
2.0
1.8
MICROCOPY RESOLUTION TEST CHART
NATIONAL BUREAU OF STANDARDS 1963 A

Report SR81-R-4529-02

Erosion Mechanisms of Metals

M.E. Guiden and K.G. Kubarych

Solar Turbines Incorporated
2200 Pacific Highway
San Diego, California 92138

30 November 1981

Annual Report for Period 1 October 1980 — 30 September 1981

Unclassified - Distribution Unlimited

Prepared for
DEPARTMENT OF THE AIR FORCE
OFFICE OF SCIENTIFIC RESEARCH
Bolling Air Force Base, DC 20332

NOTICE

This document was prepared under the sponsorship of the Air Force. Neither the U.S. Government nor any person acting on behalf of the U.S. Government assumes any liability resulting from the use of the information contained in this document.

...ment (AFSC)

AIR FO...
NOTI...
This ... is
app...
Distrib...
MATTHEW J. K...
Chief, Technical Information Division

UNCLASSIFIED

SECURITY CLASSIFICATION OF THIS PAGE (When Data Entered)

REPORT DOCUMENTATION PAGE		READ INSTRUCTIONS BEFORE COMPLETING FORM
1. REPORT NUMBER AFOSR-TR- 82-0080	2. GOVT ACCESSION NO. AD-A111 537	3. RECIPIENT'S CATALOG NUMBER
4. TITLE (and Subtitle) EROSION MECHANISMS OF METALS		5. TYPE OF REPORT & PERIOD COVERED Annual 10/1/80 - 9/30/81
		6. PERFORMING ORG. REPORT NUMBER SR81-R-4526-02
7. AUTHOR(s) Kenneth G. Kubarych and Mary E. Gulden		8. CONTRACT OR GRANT NUMBER(s) F49620-78-C-0104
9. PERFORMING ORGANIZATION NAME AND ADDRESS Solar Turbines Incorporated 2200 Pacific Highway, P.O. Box 80966 San Diego, California 92138		10. PROGRAM ELEMENT, PROJECT, TASK AREA & WORK UNIT NUMBERS 61102F 2306/A2
11. CONTROLLING OFFICE NAME AND ADDRESS Department of the Air Force Office of Scientific Research Bolling Air Force Base, DC 20332		12. REPORT DATE November 1981
		13. NUMBER OF PAGES 37
14. MONITORING AGENCY NAME & ADDRESS(if different from Controlling Office)		15. SECURITY CLASS. (of this report) Unclassified
		15a. DECLASSIFICATION/DOWNGRADING SCHEDULE

16. DISTRIBUTION STATEMENT (of this Report)

Approved for public release; distribution unlimited.

17. DISTRIBUTION STATEMENT (of the abstract entered in Block 20, if different from Report)

18. SUPPLEMENTARY NOTES

19. KEY WORDS (Continue on reverse side if necessary and identify by block number)

Metals
Dust Erosion
Solid Particle Impact
Strain Rate
High Carbon Steel
Microstructure
Scanning Electron Microscopy

20. ABSTRACT (Continue on reverse side if necessary and identify by block number)

The objective of this program is to identify the material properties which control erosion, as well as the material removal process. Based on previous experimental work, an erosion model has been hypothesized and is based on the target stress-strain response beneath the impacting particle. At low particle energies only elastic strain is generated and no damage to the target occurs. At higher energies, the peak stresses increase, leading to brittle fracture or plastic deformation accompanied by adiabatic heating. If adiabatic heating occurs, three possibilities arise. One is a temperature

cont

DD FORM 1 JAN 73 1473 EDITION OF 1 NOV 65 IS OBSOLETE

UNCLASSIFIED

SECURITY CLASSIFICATION OF THIS PAGE (When Data Entered)

increase with no loss of material, and the second is that ductile fracture may occur due to inadequate ductility at whatever temperature is reached. The third is that localized regions attain the melting point prior to ductile fracture.

A complete relationship exists between strain rate, adiabatic heating, and erosion rate. Erosion rate experiments using various particle sizes and velocities and target materials were performed in order to study this relationship. Target materials of 1095 steel, 2024 aluminum and pure molybdenum, copper, and gold were used as well as three Fe-Cr binary alloys.

Typically, erosion rates were greater for large particle (940 micron) erosion and at incidence angles of 30 degrees. Heat treating the steel and aluminum target materials influenced erosion rates when large particles were used, but had little influence for small particles. Additionally, erosion at 30-degree impingement shows little influence by heat treatment for either large or small particles. Evidence of adiabatic heating was found by examining the eroded surfaces of the target materials.

Tentative explanations of the erosion response to varying particle size and heat treat conditions are based on the strain rate during the impact event. Erosion rate is apparently related to the dynamic strength of the target materials.

A

TABLE OF CONTENTS

LIST OF FIGURES

LIST OF FIGURES (CONT)

1

INTRODUCTION

The erosion of metals by gases containing solid particles occurs in a large number of circumstances where performance and life of Air Force systems are severely affected. The erosion of aircraft skins during low level flight through sand storms, and the erosion of metallic components in the gas turbine power plant provide common examples of erosion. The need to understand erosion of metals is made greater by the trend to materials with marginal ductility, such as the titanium aluminides, where a wider spectrum of erosion mechanisms may be expected. An understanding of erosion mechanisms is also necessary before modification of materials to improve erosion resistance can be made.

Over the past 20 years many models have been proposed for erosion of metals. However, none of them explain or predict erosion behavior of a wide variety of metals and erosion conditions. One of the primary reasons for the inadequacy of the models is that erosion is a "dynamic" process and many of the quasi-static target properties such as flow stress and hardness are changing rapidly during particle impact. The approach taken in this program is to develop a model based on the stress-strain response beneath the impacting particle. It has become increasingly clear that the original model, although valid in principle, must be expanded to incorporate interdependent target properties which vary during the erosion process.

This is the third annual report on an on-going program to investigate the erosion mechanisms of metals and to develop a predictive model for erosion of metals. Due principally to the high strain rates and short dwell times during impact, conventional mechanical properties are not sufficient to explain erosion behavior for conditions which simulate a dust erosion environment. Strain rates during impact are dependent on both particle size and velocity. Under certain conditions, strain rates during impact on the order of 10^6/sec are expected (Ref. 1). Information on the behavior of metals at these high strain rates is limited, but existing data does show a linear variation of flow stress with strain rate, i.e., viscous flow at strain rates greater than 10^3/sec (Ref. 2). Further evidence that conventional deformation mechanisms are not necessarily rate controlling for metallic erosion is that erosion of pure metals is more a function of the energy required to melt a unit volume than of static hardness or flow stress. Other basic properties such as bond energy also show good correlation with erosion of pure metals (Refs. 3 and 4). Due to the short dwell times of impact, on the order of 10^{-6} second, the deformation is essentially adiabatic and localized temperature increases are expected. The appearance of erosion debris and impact damage has suggested that localized melting may also be a significant contributor to erosion under certain conditions (Refs. 5 thru 8).

The above brief discussion illustrates the complexity of the erosion process. The approach taken in this program to elucidate erosion mechanisms is to assume that erosion is related to the target stress-strain response beneath the impacting particle. Based on this assumption, a series of events can be postulated based on particle energy transfer. In simple terms, at low particle energies only elastic strain is generated and no permanent damage to the target occurs. At higher energies, the peak stresses increase, leading either to brittle fracture or to plastic deformation accompanied by adiabatic heating. If adiabatic heating occurs, three possibilities arise. One is a temperature increase with no loss of material, the second is that ductile fracture occurs due to inadequate ductility at whatever temperature is reached. The third is that localized regions attain the melting point prior to ductile fracture.

The original approach of using a single target material which can be heat treated to a wide range of conditions ranging from brittle to very ductile has been expanded to include materials that incorporate both microstructural variations and "lattice" type changes. The term lattice is used to mean fundamental characteristics associated with atomic bonding, i.e., bond energy, modulus of elasticity, etc. This is a necessary complication due to the fact that erosion occurs at very high strain rates and for very short durations. Hutchings (Ref. 9) concludes that conventional microstructural strengthening mechanisms become less effective as strain rates increase based on data with strain rates up to 10^3-10^4/sec. Strain rates in erosion are typically 10^5-10^7/sec clearly indicating a need for characterizing erosion of materials in addition to conventionally heat treated alloys.

The first year results on this program revealed that of the five high carbon steels investigated, three exhibited a transition from brittle to ductile type erosion as a function of heat treatment for test conditions which simulate a dust erosion environment (quartz particle impact). Depending on heat treatment ranging from fully hardened to over-tempered martensite, erosion weight loss varied by a factor of four for 90-degree impingement. A minimum high value of hardness or flow stress is required to produce a brittle erosion response (maximum erosion at 90 degrees). However, for 30-degree impingement there was no significant difference in erosion for various heat treat conditions. The transition from brittle to ductile erosion behavior is also dependent on impacting particle size. Regardless of heat treatment, only ductile response was produced for impact with 10 micron particles. Examination of single impacts revealed that damage for brittle type erosion response was not characterized by brittle fracture, but rather by intense localized plastic flow producing lips around the crater periphery. Plastic strain was less localized and shear lip formation was minimized for the softer, lower stress heat treat condition.

Experiments throughout the second year were designed to further clarify the observation made during the previous year. Examination of both the eroded surfaces and of single impacts revealed no evidence of brittle fracture, but rather an increase in localized plasticity with increasing target hardness. Also, the target materials with the highest hardness showed evidence of transformation whereas the softer materials showed none. The transformation products occur in the extruded shear lips and subsurface along regions of maximum shear stress and are the result of adiabatic heating. The variation in amount

of transformation with target hardness is probably due to the distribution of the strain during impact, i.e., the local instantaneous strain rate. This is also suggested by the observation that plasticity increased with decreasing particle size, since the smaller the particle the higher the strain rate keeping velocity constant. Erosion behavior of Ti_3Al also showed plasticity and transformation products were observed for the most brittle material, similar to the 1095 steel.

The emphasis in this year's work was to separate and identify the contribution of (1) adiabatic heating which decreases flow stress, and (2) increasing strain rates, which increases flow stress on the erosion processes. An understanding of these competing processes is necessary to develop an erosion model and define the target properties which control erosion response. Further analyses of the 1095 steel targets, and testing and analyses of additional metallic targets is being done to accomplish these objectives.

2

EXPERIMENTAL PROCEDURES

2.1 MATERIALS

Several target materials were investigated; the SAE 1095 steel and the 2024 aluminum were heat treated to various conditions, while the pure materials OFHC copper, molybdenum, 24 kt gold, and pure iron were tested in the annealed condition. Two Fe-Cr alloys (Fe-20wt%Cr and Fe-30wt%Cr) were prepared by vacuum arc melting. These alloys exhibit significant solid solution hardening yet are single phase alloys. The alloys were erosion tested in the as-cast condition. The 1095 steel was erosion tested in the quenched and tempered condition. The general heat treating procedure consisted of normalizing all specimens, then heating to above the austenitizing temperature (782°C) in a purified argon atmosphere and brine quenching. All specimens were tempered in boiling water which produces maximum hardness and eliminates the spontaneous cracking which occasionally occurs with the untempered material. To obtain desired tempered hardness specimens were heated in argon to various temperatures below the austenite transformation temperature. The 2024 aluminum is an age-hardeneable alloy, hardening is produced primarily by precipitation of the intermetallic phase θ' (i.e., $CuAl_2$). The materials were treated to three standard conditions 2024-0 furnace annealed, 2024-T3 solution treated, and 2024-T81 precipitation hardened. Typical mechanical properties of the materials tested are shown in Table 1.

Specimens were chemically milled 0.02 cm after heat treatment to remove any scale or decarburized material. The specimens were again immersed in boiling water to remove any hydrogen introduced during the chemical milling treatment.

This rather elaborate specimen preparation procedure was considered necessary to produce consistent, well characterized target material.

Two particle compositions were used for erosion testing: natural quartz sand and SiC. Quartz sand was chosen because in previous work it was found to be the principal erosive component in natural dusts, i.e., the amount of erosion was directly proportional to the percentage of quartz in the natural dusts (Ref. 5). The dust size ranges were chosen to be representative of airborne dust and to provide significant mass differences.

A single particle size range of SiC was used (660-1346 microns) to provide a significant increase in particle energy, and attendant strain rate decrease. Typical erosion test conditions are given in Table 2.

Table 1

Target Properties

Material	σ_y (MPa)	σ_{Shear} (MPa)	E (GPa)	Hardness (GPa)	Density (gm/cm^3)
2024Al-0	76	120	73	0.6	2.77
-T3	340	280	73	1.5	2.77
-T81	450	280	73	1.6	2.77
OFHC Copper	140	-	117	0.7	8.92
Molybdenum	570	-	324	2.0	10.2
Gold	-	-	79	-	19.32
Iron	-	-	207	-	7.84
1095 Rc66	2070	-	207	8.5	7.84
1095 Rc20	590	-	207	2.4	7.84

Room temperature values

Table 2

Erosion Test Conditions

Angle of Impingement	Particle Size (microns)	Particle Velocity (mps)
90°	10	300, 152, 61
	136	213, 152, 50
	273	188, 152, 44
	940	132
60°	10	300
	136	152
	273	152
30°	10	300, 152, 61
	136	213, 152, 50
	273	188, 152, 44
	940	132

2.2 EROSION TESTING

Erosion tests were performed with a stationary target impacted by particles accelerated in an air stream. Particles are injected into the stream three meters from the target to provide sufficient distance for acceleration. The air velocity variation across the 0.95 cm diameter nozzle is less than five percent and velocity can be varied between 15 and 343 m/sec to achieve the desired particle velocity. Particle velocity is measured using the rotating double disc technique (Ref. 10). Particle velocities of 300, 188, 152, 120 and 61 mps for each particle size range were used to establish erosion rates and determine the particle size and velocity dependence on erosion. The particles are fed into the gas stream using a precision feeder at a sufficiently low concentration that particle interactions in the carrier gas stream or on the target surface are negligible.

To assess the type of erosion (brittle or ductile) tests were performed at 30, 60 and 90 degree impingement angles. The number of particles per test was varied from a few particles (to examine single particle impacts and incubation effects) to as many as 10^{11} particles (400 grams of dust) over a 0.75 cm^2 target area. For long time tests with a large number of particles the specimens were weighed at specific intervals to assess any changes in erosion with number of impacts. All tests were performed at ambient temperature. In most cases, tests were performed in triplicate to assure reproducibility of the data.

2.3 EXAMINATION OF ERODED SURFACES

The eroded surfaces and single impacts were examined both optically and by scanning electron microscopy (SEM). The energy dispersive X-ray attachment on the SEM was used to detect silicon which would indicate the presence of quartz or SiC particle residue. The surfaces were also examined in cross section to assess the nature of subsurface damage.

3

EXPERIMENTAL RESULTS AND DISCUSSION

3.1 FURTHER ANALYSIS OF 1095 STEEL TARGETS

The 1095 steel targets heat treated to hardness levels ranging from Rc 20 to Rc 66 exhibit an apparent transition from brittle to ductile type erosion behavior, as evidenced by a change in angle of maximum erosion from 90 to 30 degrees. However, the eroded surfaces did not exhibit features of brittle fracture, but rather increasing plasticity with increasing initial hardness or flow stress. This plasticity is evidence of significant adiabatic heating. Subsurface microstructural transformation bands formed during erosion are additional evidence of adiabatic heating to at least 800°C in these localized regions.

Evidence of melting in the form of discrete spherical iron particles attached to the target surface after erosion have been observed. Recent examination of erosion debris particles confirm the existence of melting during erosion. Small spherical drops of iron (determined by scanning electron microscope [SEM] - X-ray analysis) are routinely observed attached to the much larger erosion debris particles on targets heat treated to high hardness levels. An example is shown in Figure 1. In addition to the spherical droplets other evidence of melting or incipient melting is seen in the flatish droplets on the surface. In this particular case, molten material per se does not contribute significantly to erosion weight loss, but may contribute to the likelihood that the erosion debris particle will detach from the target. The melting may occur during particle impact due to adiabatic heating in the subsurface maximum shear stress band (corresponds to transformation and deformation zones seen in cross section) or as the erosion debris particles detach due to adiabatic plastic deformation and friction.

Additional evidence of significant adiabatic heating in the hard 1095 steel targets exists in the form of the dimpled structure observed on erosion debris particles. An example is shown in Figure 2. This dimpled structure is typical of ductile overload fracture and would not be expected on fracture surfaces of the low ductility as-heat treated material.

The formation of subsurface transformation bands (Fig. 3), indicative of temperature excursions to at least 800°C, is a function of both heat treatment and impacting particle size. Prerequisites for transformation are a certain high level of initial flow stress or hardness combined with sufficient particle kinetic energy. For example, after erosion with 385 micron quartz particles traveling at 150 mps, transformation bands are observed in targets of hardness

A. Erosion Debris Particle (Magnification: 660X)

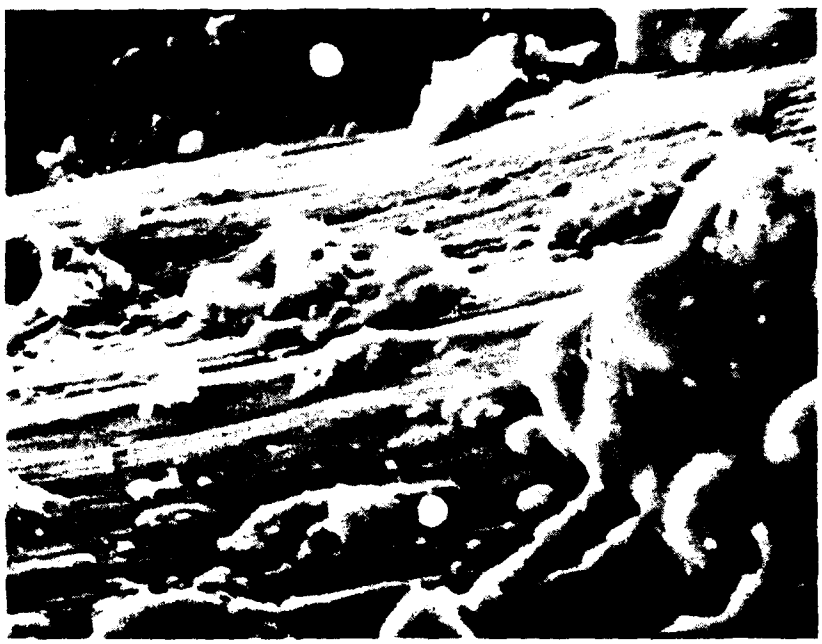

B. Details on Surface. Spherical Droplets are Evidence of Melting During Erosion. (Magnification: 5350X)

Figure 1. Erosion Debris Particle From 940 Micron SiC Impact at 90-Degree Impingement and 132 mps 1095 Steel Target Heat Treated to Maximum Hardness

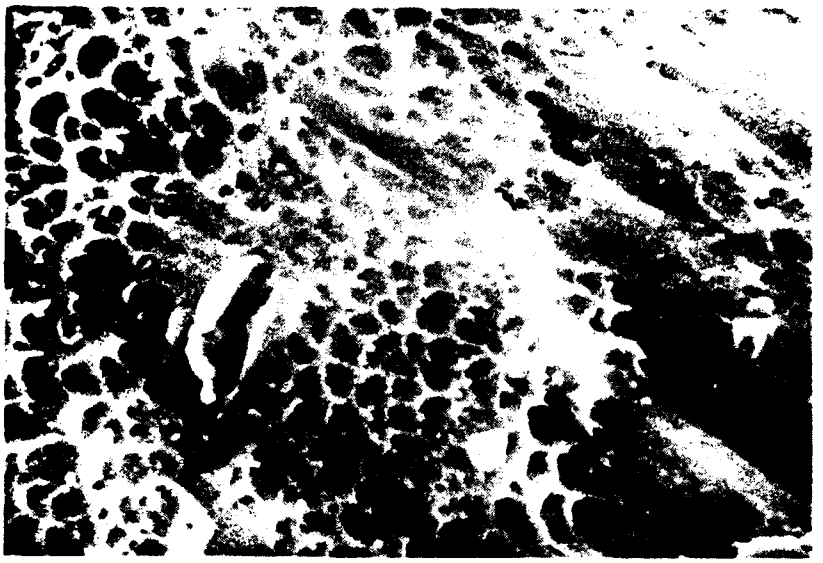

Figure 2. Dimpled Structure Characteristic of Ductile Overload Fracture Observed on Erosion Debris Particle From 1095 Steel Target in Maximum Hardness Condition. Erosion Condition - 940 Micron SiC, 90-Degree Impingement, 132 mps Velocity. (Mag: 10,000X)

as low as Rc 50 and all harder targets. On the hardest target (treated to Rc 66) transformation bands are observed after erosion with particles $\geq$163 microns. Smaller particles do not produce transformation or deformation bands.

3.2 EROSION OF ALUMINUM, COPPER, MOLYBDENUM AND GOLD

2024 aluminum alloy, OFHC copper, pure molybdenum and 24 kt gold targets have been eroded under various conditions. The 2024 aluminum targets were heat treated to provide three levels of hardness or flow stress. The erosion volume loss for 50 grams of dust is shown in Figures 4, 5 and 6 for 940 micron SiC, 273 micron quartz and 10 micron quartz particle impact. 1095 steel targets in the maximum hardness and Rc 20 heat treatments are also included. All of the new targets exhibited higher erosion at 30-degree than at 90-degree impingement, which is typical of ductile metals. The 2024 aluminum alloy in all three heat treatments generally eroded more than the other targets, and the specimens heat treated to a higher yield or flow stress eroded more than the softer fully annealed aluminum; however, the erosion rate difference between the three alloy conditions becomes less with reduced particle size.

Examples of the subsurface damage produced during erosion of the 2024 aluminum for each of the three microstructural conditions are shown in Figure 7 with the impact conditions of 273 micron particles traveling at 152 mps and at normal incidence. The depth of damage is greater on the soft 2024-0 target

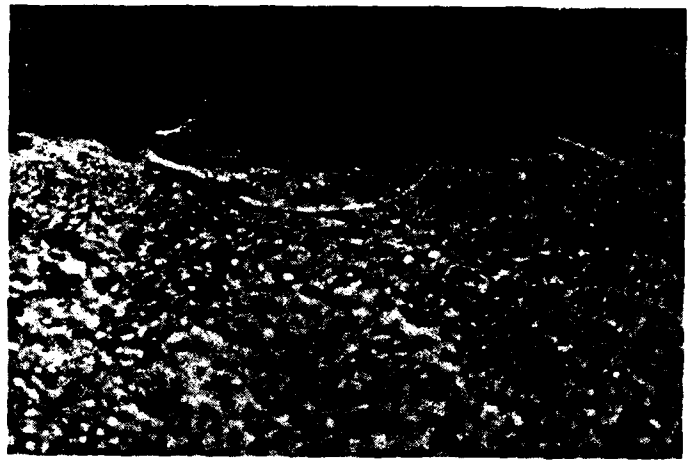

A. Rc 48, 385 Micron Quartz, 90-Degree Impingement, 152 mps Velocity

B. Rc 21, 273 Micron Quartz, 90-Degree Impingement, 152 mps Velocity

Figure 3. Optical Micrographs of 1095 Steel Showing Subsurface Transformation Band Indicative of High Temperature Exposure (Magnification: 1000X)

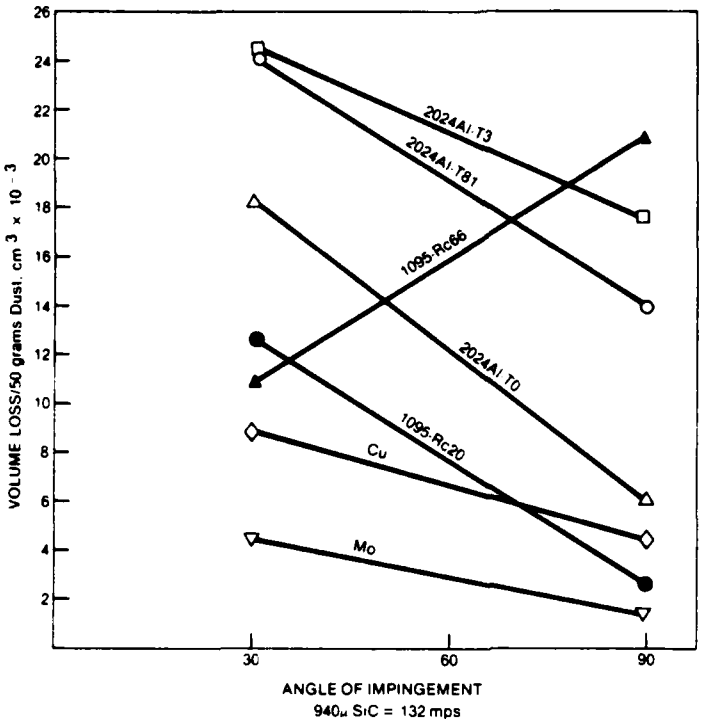

Figure 4.

Erosion Loss for 940 Micron Impact

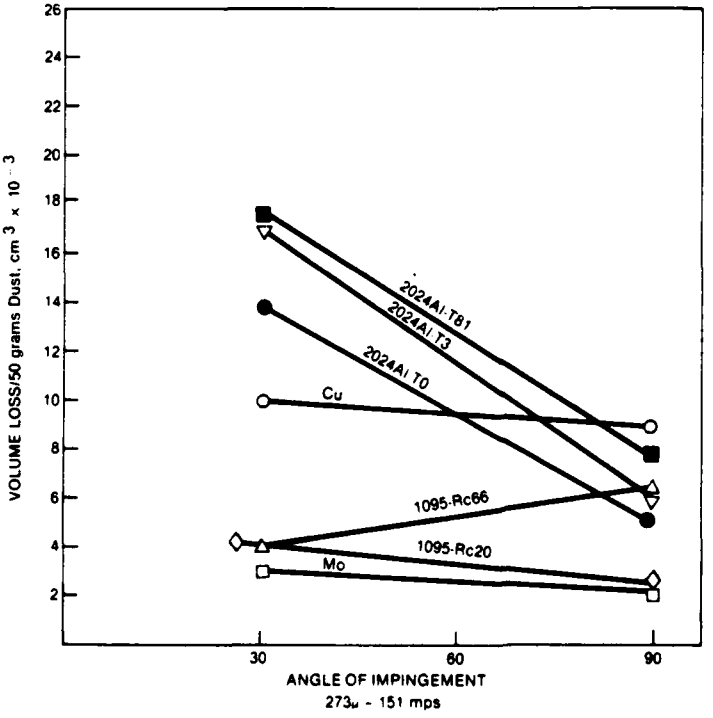

Figure 5.

Erosion Loss for 273 Micron Impact

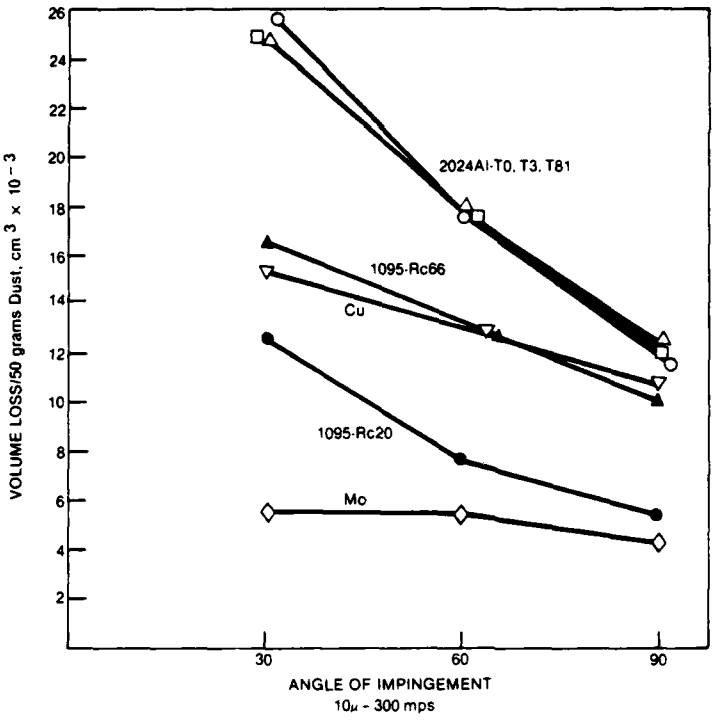

Figure 6.

Erosion Loss for 10 Micron Impact

but all three show significant damage. Adiabatic heating may lead to some dissolution of the precipitate phase. The surface layer of the specimen shown in Figure 6B indicates a change in microstructure when compared to the bulk material. Due to the extremely fine nature of the precipitate phase (the diameter of the θ' phase is approximately 10,000 mn), it would be necessary to use transmission electron microscopy to directly observe the phenomenon.

Of the three pure metals, molybdenum showed the best erosion resistance, copper the worst and gold fell in the middle. Typically, the three pure metals showed better erosion resistance than the 2024 aluminum alloy.

Figures 8 and 9 illustrate the type of subsurface damage sustained by the three materials, 2024 aluminum, copper and molybdenum, after erosion by 273 micron quartz particles traveling 152 mps. Significant damage is observed; in fact, the molybdenum having the best erosion resistance exhibits the greatest extent of damage.

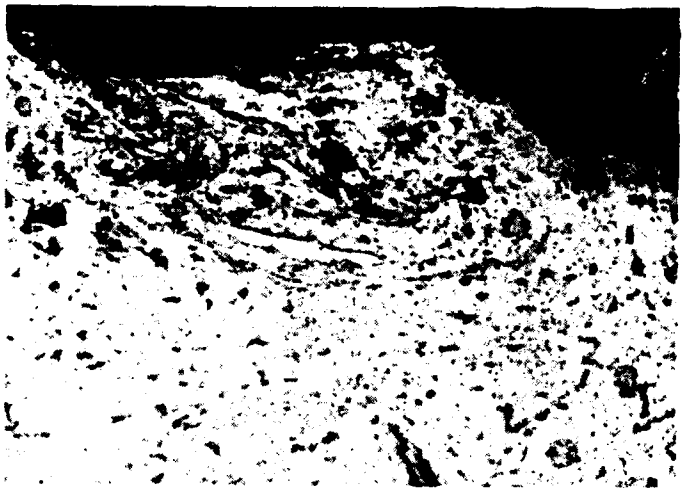

A. TO Heat Treatment
Rb 7 Hardness

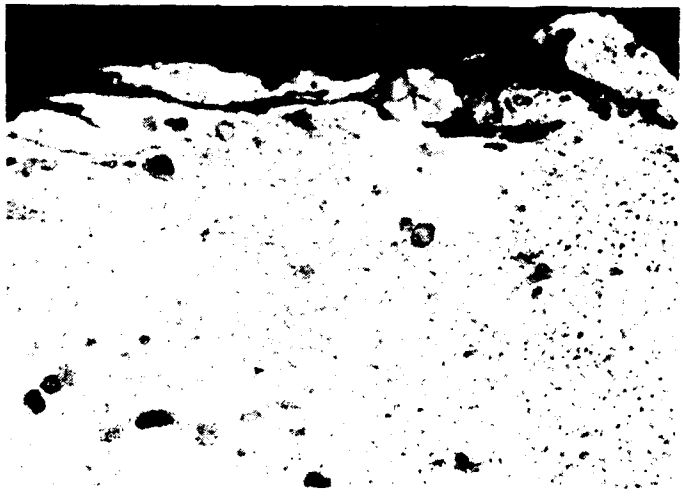

B. T3 Heat Treatment
Rb 78 Hardness

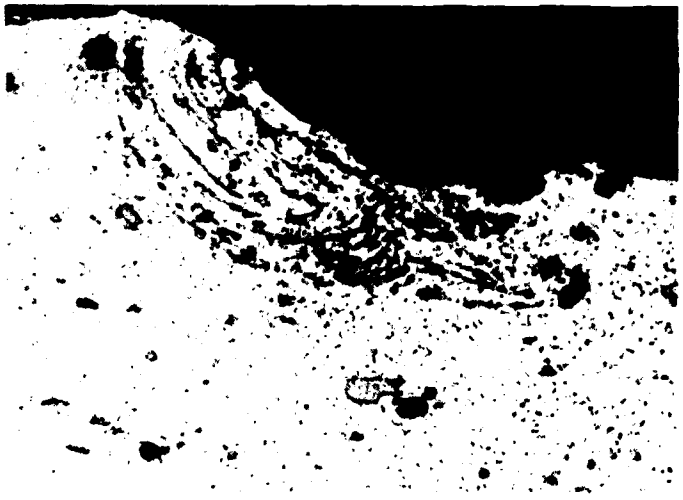

C. T81 Heat Treatment
Rb 81 Hardness

Figure 7. 2024 Aluminum Alloy Eroded With 273 Micron Quartz at 152 mps, 90-Degree Impingement (Magnification: 1000X)

Figure 8.

Copper Eroded With 273 Micron Quartz at 152 mps, 90-Degree Impingement

Magnification: 1000X

Figure 9.

Molybdenum Eroded With 273 Micron Quartz at 152 mps, 90-Degree Impingement

Magnification: 1000X

3.3 EROSION OF Fe-Cr BINARY SINGLE PHASE ALLOYS

Pure iron and two Fe-Cr binary alloys were erosion tested to investigate the effect of solid solution strengthening on the erosion behavior. Figure 10 shows the variation of erosion rate and hardness with composition. A ductile erosion response is observed since in each case erosion is greater at 30-degree impingement than at 90-degree impingement. Contrary to the age hardened alloys, the solution hardened alloys show improved erosion resistance with increased hardness.

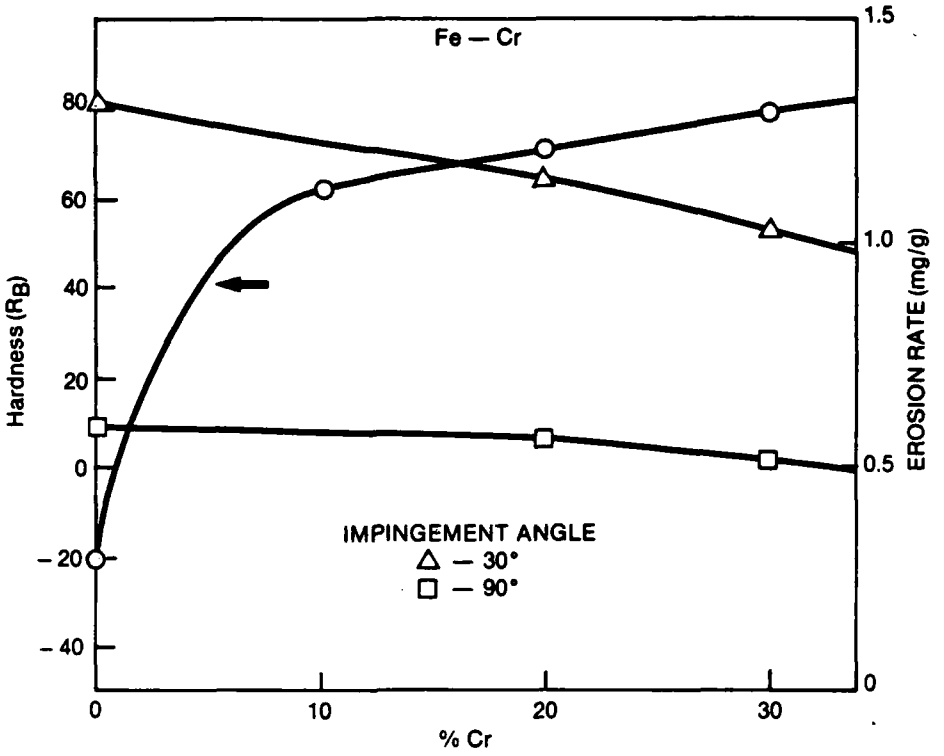

Figure 10. Variation of Hardness (Rb) and Erosion Rate With Composition. Erosion Conditions were 273 Micron Quartz Traveling at 188 mps.

3.4 SINGLE IMPACTS

Single impact erosion tests were performed on 1095 steel, copper and molybdenum targets. Figure 11 shows the impact crater of the 1095 steel target in the fully hardened condition (Rc 66). Significant flow is observed, in fact, a large shear lip is present. Again, this is evidence of an increase in ductility during the impact event. Figure 12 shows the impact damage of a copper target after simple impacts with 940, 273 and 10 micron particles. A great amount of ductility is apparent from the dimpled rupture type of fracture. Shear lips are observed for the 10 micron eroded material but for the 940 and 273 micron material, shear lips were not observed. Similarly, the molybdenum target, Figure 13, exhibited erosion damage of the same nature as copper, i.e., dimpled rupture fracture surfaces and limited observations of shear lips.

3.5 GENERAL DISCUSSION

One of the objectives of this year's efforts was to identify the effects of adiabatic heating in comparison to the effects of strain rate. Three major effects were associated with adiabatic heating: localized melting; ductile

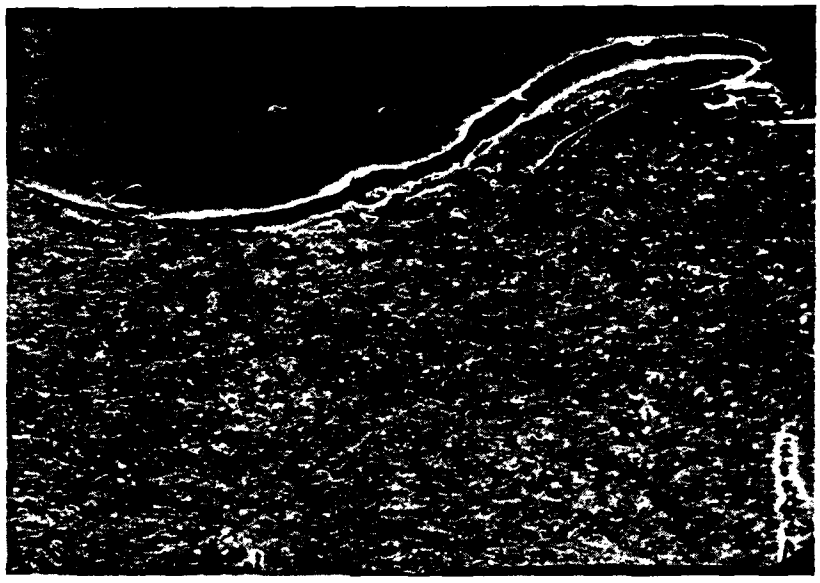

A. Magnification: 500X

B. Magnification: 1500X

Figure 11. SEM Micrograph of Single Impact Crater in Cross-Section, 1095 Steel Target, Rc 66, 940 Micron SiC Particle, 125 mps, 90-Degree Impingement

A. 940 Micron SiC

Mag: 300X

B. 273 Micron Quartz

Mag: 770X

C. 10 Micron Quartz

Mag: 5500x

Figure 12. SEM Micrographs of Single Impact Craters of a Copper Target

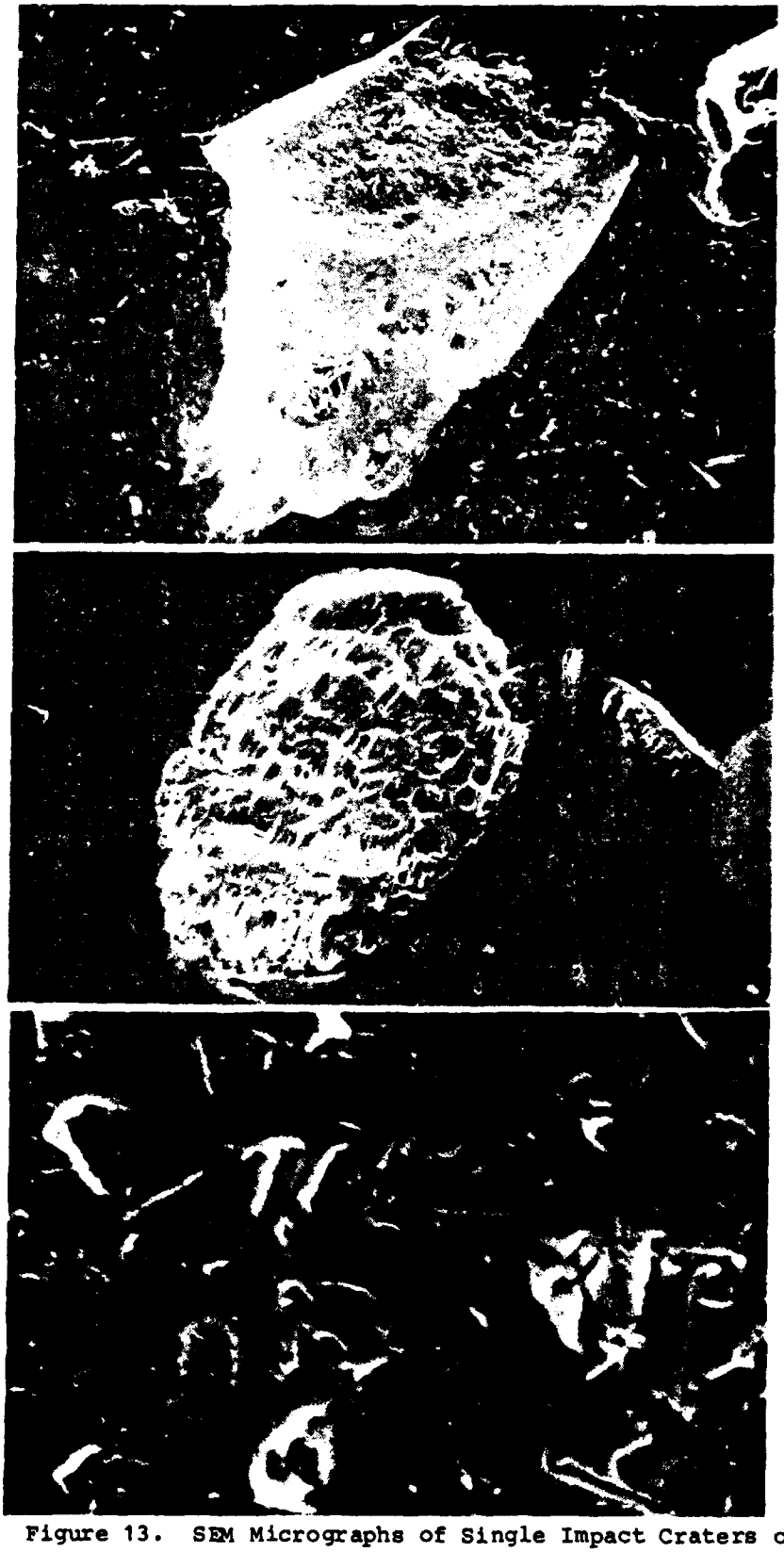

A. 940 Micron SiC

Mag: 200X

B. 273 Micron Quartz

Mag: 650X

C. 10 Micron Quartz

Mag: 6000X

Figure 13. SEM Micrographs of Single Impact Craters of a Molybdenum Target

fracture of a brittle target material; and formation of subsurface transformation bands. Melting was observed with the 1095 steel targets in the fully hardened condition. Ductile, dimpled rupture fracture surfaces were observed for all eroded materials regardless of their heat treat condition. Transformation bands were observed as a function of both heat treatment and particle size. These observations indicate a complex interrelationship between adiabatic heating and strain rate. The competing effects of heating and strain rate are illustrated in Figures 14 and 15 for mild steel and molybdenum. As the temperature increases the strength decreases for all strain rates while increasing the strain rate increases the strength for all temperatures.

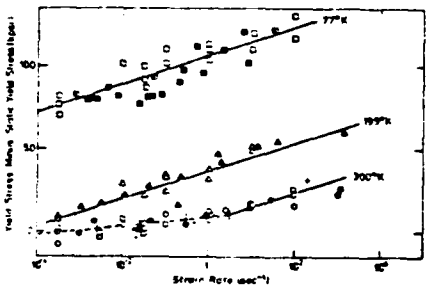

Figure 14.

Temperature and Strain Rate Dependence of the Lower Yield Stress of Mild Steel (Data of Ref. 11, Figure Taken From Ref. 2)

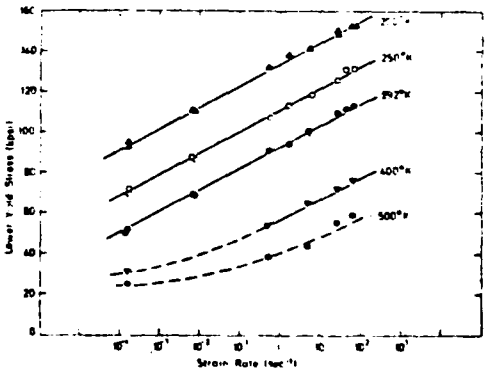

Figure 15.

Temperature and Strain Rate Dependence of the Lower Yield Stress of Molybdenum (Data of Ref. 12, Figure Taken From Ref. 2).

Strain rate is a function of both particle size and velocity. The calculation by Hutchings (Ref. 1, Fig. 16) estimated the mean strain rate as a function of both particle size and velocity. The range of particle sizes used in this program varied from 10 to 940 microns and velocities varied from 50 to 1000 mps. This results in a variation of the mean strain rate from 10^4 to 10^7/sec, all well above the strain rates at which mechanical properties are ordinarily measured. This is the complication of correlating a material property with erosion resistance. Very little data exists at such high strain rates and the material response during these very brief events of particle impact are not well understood. However, from the data gathered in this program, some comments can be made on strain rates and erosion resistance.

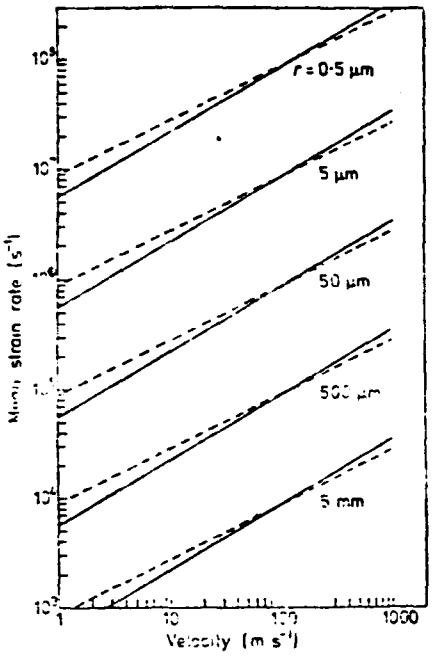

Figure 16.

Estimated Mean Strain Rates Associated With the Impact of Steel Spheres Onto a Steel Surface. Solid Lines, Purely Elastic Behavior; Broken Lines, Perfect Plastic Behavior (Ref. 1)

Figures 17 through 21 show the erosion data plotted versus the particle size, keeping particle velocity, impact angle and material condition constant. Considering the results shown in Figure 16, the particle size is analogous to strain rate, the 10 micron particle corresponds to a strain rate of approximately 5 x 10^6/sec, whereas the 940 micron particle corresponds to a strain rate of approximately 5 x 10^4/sec. For each material tested the erosion rate decreased with decreasing particle size, implying that erosion rate decreases with increasing strain rate. This can be rationalized with the help of Figures 14 and 15. As the strain rate increases the strength of the material increases monotonically. Therefore, at the high strain rates associated with the small particle sizes the dynamic response of the target material results in a stronger, more erosion resistant material. Also associated with the high strain rates are very short loading times, resulting in a reduction in the duration of the event. This could possibly reduce any effects due to adiabatic heating through reduced heat transfer, resulting in increased erosion resistance. One other aspect of the reduced erosion rate versus particle size could be an effect of failure of the quartz particles due to shock loading. Failure of the quartz would reduce the amount of energy available to inflict erosion damage in the target material, thereby reducing the erosion rate.

The influence of material condition as a function of particle size (i.e., strain rate) is demonstrated in Figures 17 and 18. For large particles a large variation in erosion rate occurs with the various heat treat conditions, whereas for the small particles the difference in erosion rate becomes quite small. This could be a reflection of the deformation process as related to strain rate. The large particles with the lower strain rates may behave in a more conventional sense, where microstructure and ordinary hardening

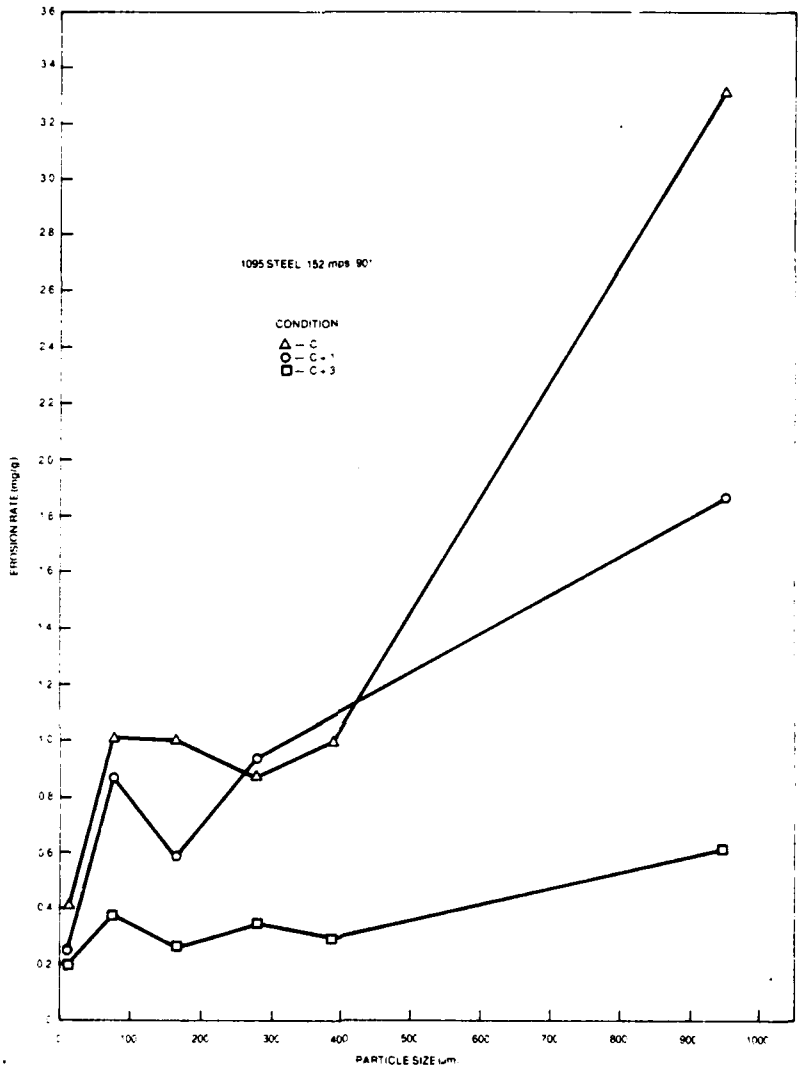

Figure 17A. Erosion Rate Versus Particle Size of 1095 Steel Heat Treated to Three Different Conditions: C-Rc66; C+1-Rc63, and C+3-Rc29.

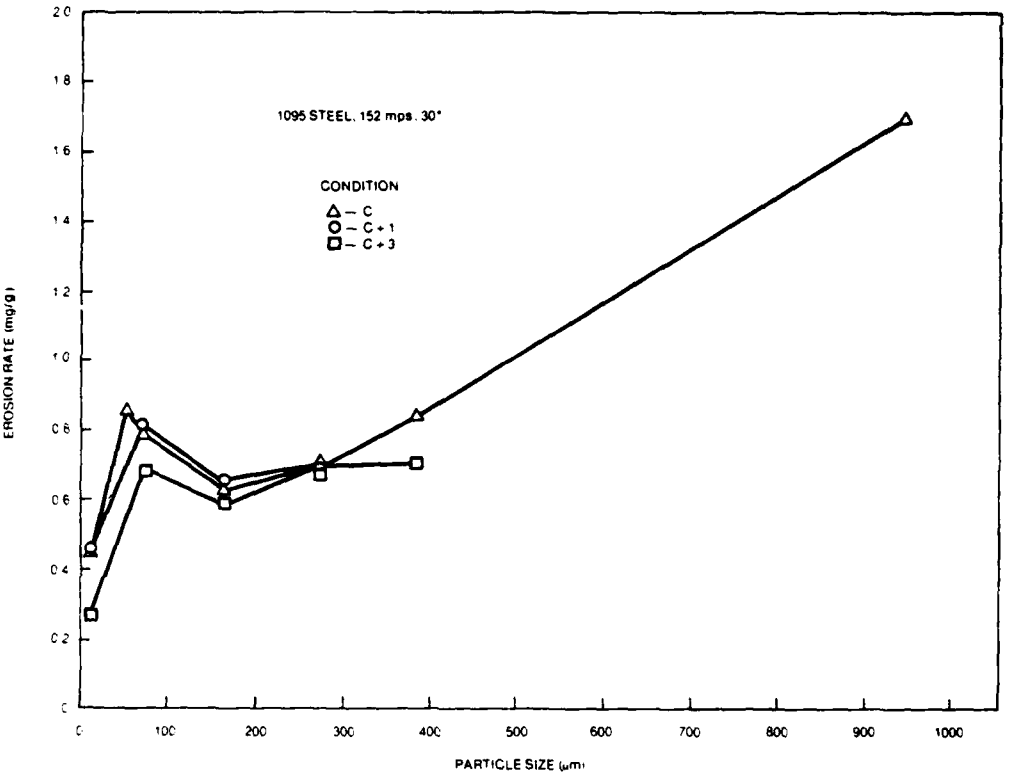

Figure 17B. Erosion Rate Versus Particle Size of 1095 Steel Heat Treated to Three Different Conditions: C-Rc66; C+1-Rc63, and C+3-Rc29.

mechanisms apply. However, with small particles and very high strain rates those conventional techniques of material processing may not be as important during the deformation event. In looking though the data presented in Figures 17 through 21, there is a variation in erosion rate from one material to another when eroded with 10 micron particles; unfortunately, at this stage it is unclear what is the controlling material parameter.

One final feature associated with the influence of particle size on the erosion rate is the apparent lack of effect of particle size on erosion rate when impingement is at 30 degrees. This is clearly shown in Figure 18B and to a lesser extent in Figure 17B. The data shows that at 30-degree angle of incidence heat treatment condition does not affect the erosion rate, even though the erosion rate is significantly affected by angle of incidence. The angular dependence is surely associated with differing erosion mechanisms at the various impintement angles and the material response to these differing mechanisms.

Pure metals as well as the steel and aluminum alloys show the same type of behavior with respect to particle size and angle of incidence. The Fe-Cr alloys, however, have an erosion behavior that deviates slightly from that

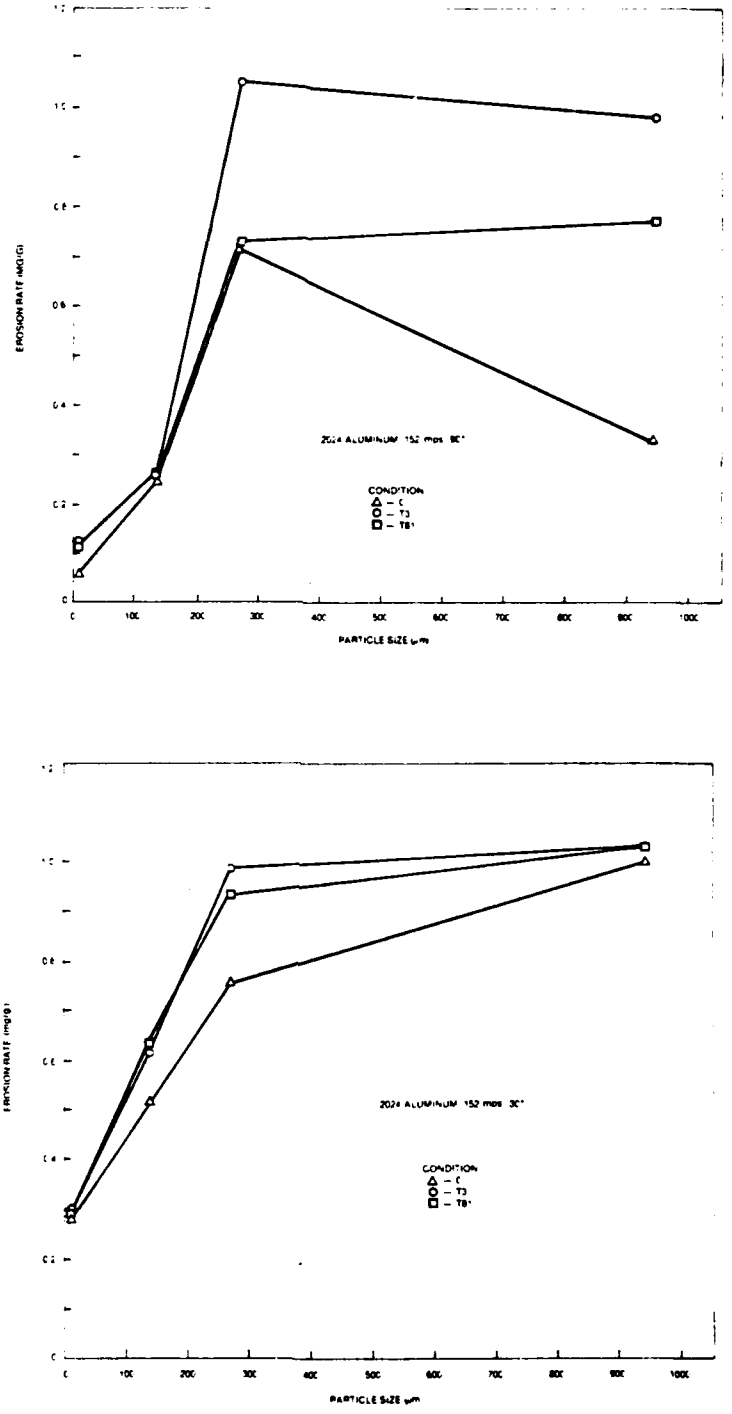

Figure 18. Erosion Rate Versus Particle Size of 2024 Aluminum Heat Treated to Three Different Conditions

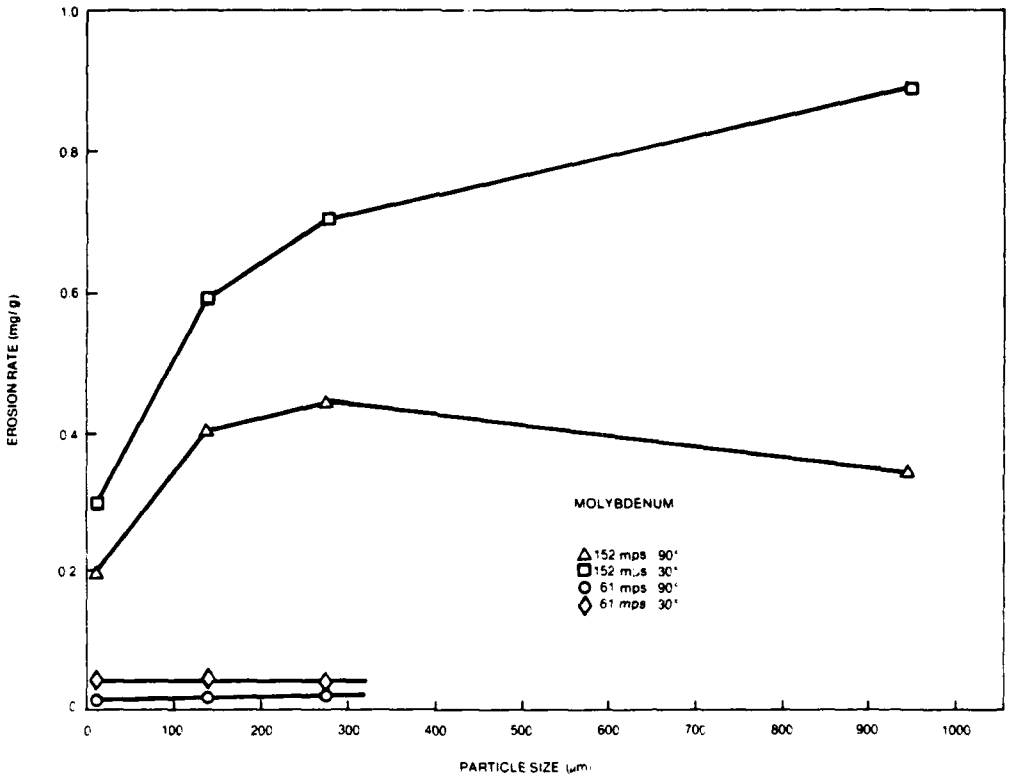

Figure 19. Erosion Rate Versus Particle Size of Pure Molybdenum

found for the 1095 steel alloy. Figure 11 shows the erosion rate of pure Fe and two Fe-Cr alloys, along with the Rb hardness. The figure shows that as the hardness of the the Fe-Cr alloys increase the erosion rate decreases. This is quite different than what was found for the 1095 steel shown in Figure 22. The erosion rate of the 1095 steel increased with increasing hardness, quite the opposite of the Fe-Cr alloy. It is true that the hardness levels of the two alloy systems are not comparable, but it is believed the effect is real and not just an artifact of the experiment. Again, it is thought to be a consequence of the dynamic strain rate response. The Fe-Cr alloys are single phase alloys which are solid solution hardened. Solid solution hardening occurs by forcing different size solute atoms into the solvent lattice, increasing the strain on the lattice. This is a fundamental change in the structure of the material; whereas, the steel is hardened primarily by the precipitation of carbides. Changing the morphology of the carbides does little to the iron matrix, in fact, precipitation of carbides reduces the amount of solute atoms dissolved in the iron lattice. Consideration of fundamental material characteristics, such as the atomic structure, must be made in order to more fully understand the mechanisms of erosion.

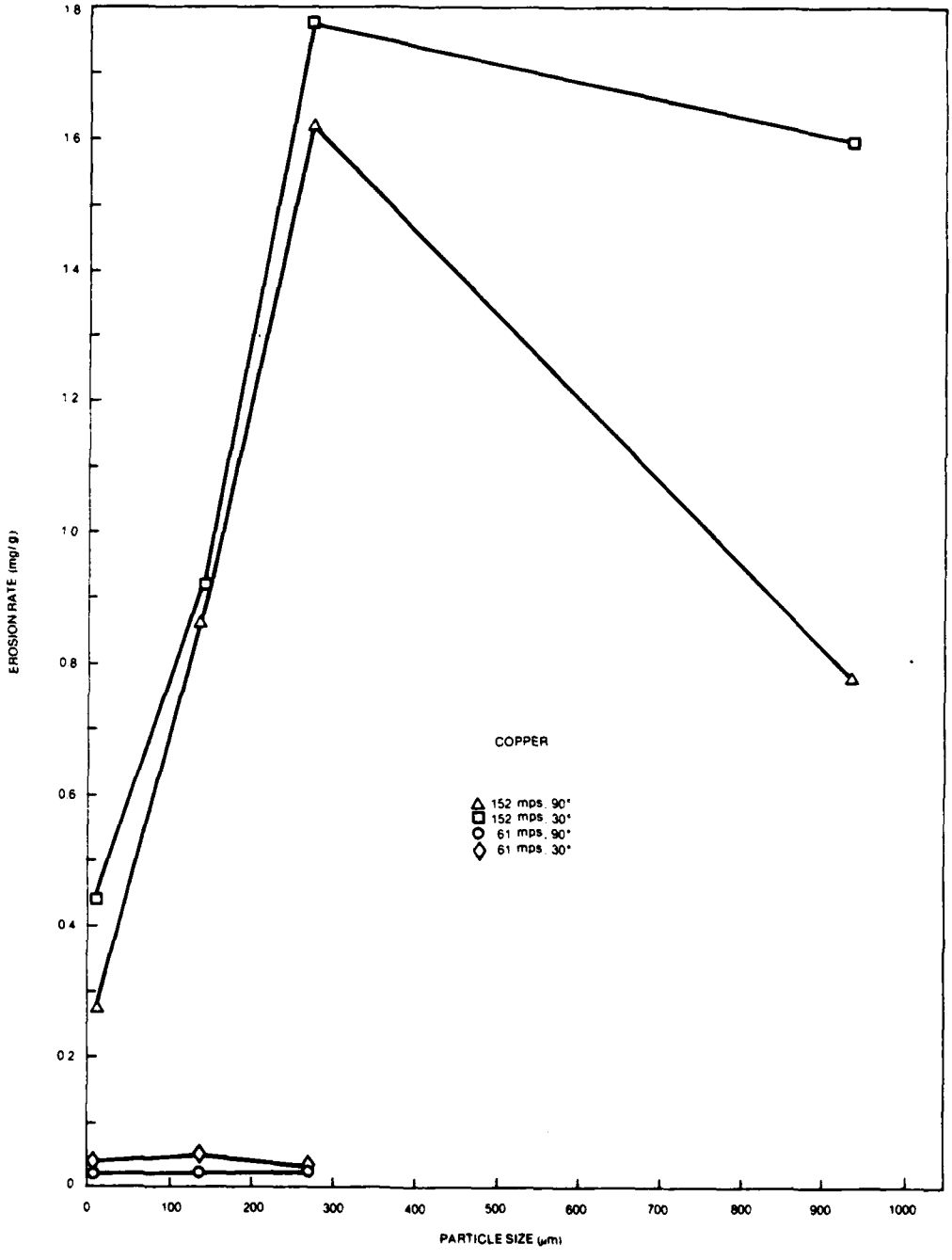

Figure 20. Erosion Rate Versus Particle Size of Pure Copper

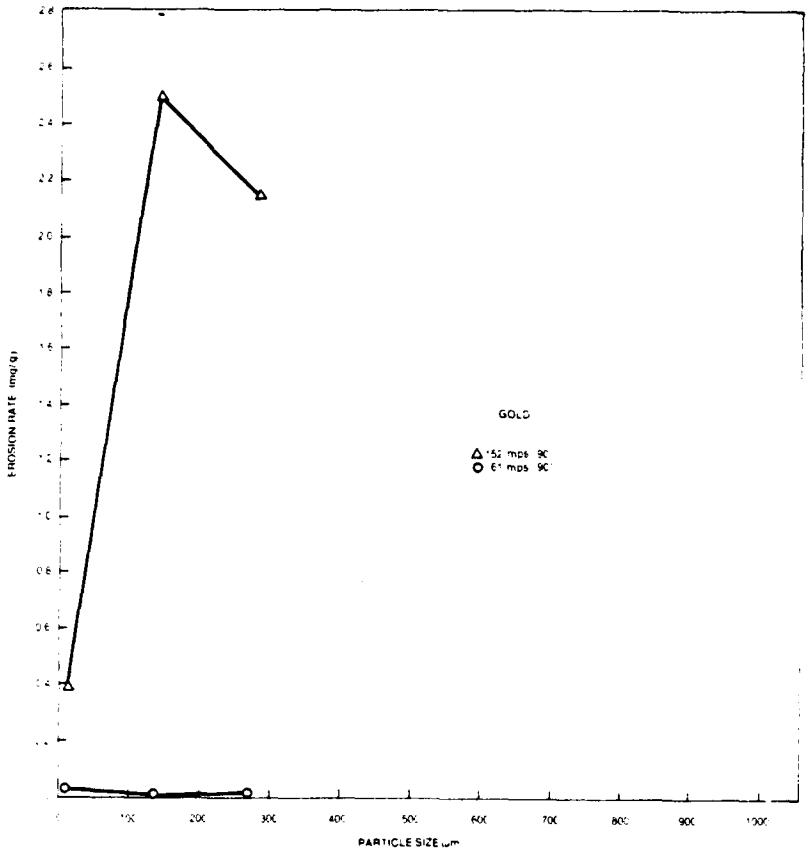

Figure 21. Erosion Rate Versus Particle Size of Pure Gold

Much of this discussion has been of a speculative nature; however, it is based on both theoretical and experimental work. The investigations during 1982 will be designed to clarify many of these points through both analytical and experimental activities. Much of the effort will be directed toward understanding high strain rate deformation and measurement of properties in the realm of these high strain rates.

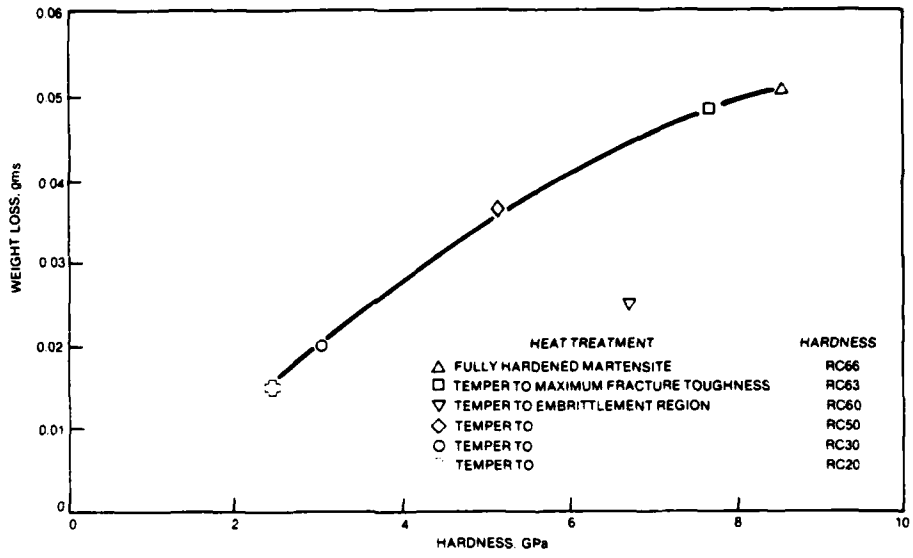

Figure 22. Erosion Weight Loss Versus Target Hardness of 1095 Steel at 90-Degree Impingement Angle (Data Taken From Ref. 13)

4

SUMMARY

The third year's results to investigate the mechanisms of solid particle erosion are presented. Target materials of 1095 steel, 2024 aluminum and pure molybdenum, copper and gold were tested. In addition, pure iron and two Fe-Cr alloys were tested because they are single phase solid solution hardened alloys. All of the materials exhibited a ductile type of erosion, i.e., erosion rate was greater at 30 degrees than at 90 degrees. Erosion rates were generally greater with 940 micron sized particles than with 10 micron particles. Molybdenum shows the best erosion resistance of all the material tested. The copper and gold were not as good as molybdenum, but better than aluminum; steel depended upon erosion conditions.

Examination of the eroded surfaces provided evidence of adiabatic heating. Localized melting, dimpled rupture fracture surfaces and subsurface transformation bands were all observed. The extent of the effect of adiabatic heating appeared to be a function of erosion conditions.

Erosion rates are a strong function of particle size. It was found that large particles impacting with relatively low strain rates are sensitive to conventional heat treatments, whereas small particles with relatively high strain rates are insensitive to conventional heat treatments. This can be related to the material response during the deformation event.

The Fe-Cr binary alloys show a very different erosion response to changing hardness than does the heat treated steel. While the steel shows an increase in erosion with increased hardness, the Fe-Cr alloys show a decrease in erosion rate with increased hardness. The difference is partially attributed to a difference in the strengthening mechanism. Steel is precipitation hardened by heat treating to produce obstacles to dislocation motion, Fe-Cr alloys on the other hand are hardened by solid solution hardening, which simply increases the strain in the lattice. For deformation at high strain rates where motion of dislocation may not be the dominant mode of plastic flow, the more highly strained lattice may resist deformation more effectively.

Much of the work during 1981 raised interesting questions on strain rates and its relationship to adiabatic heating and erosion rates. Future work will be aimed at investigating these points and at determining the rate limiting material parameters associated with the erosion mechanism.

REFERENCES

1. Hutchings, I.M., 1977, "Strain Rate Effects in Micro particle Impact", J. Phys. d: Appl. Phys., 10, pp. 151-156.

2. Campbell, J.D., 1973, "Review Paper Dynamic Plasticity: Macroscopic and Microscopic Aspects", Mat. Sc. & Eng., 12, pp. 3-21.

3. Hutchings, I.M., 1975, "Prediction of the Resistance of Metals to Erosion by Solid Particles", Wear, 35, pp. 371-374.

4. Vijh, A.K., 1976, "Resistance of Metals to Erosion by Solid Particles in Relation to the Solid State Cohesion of Metals", Wear, 39, pp. 173-175.

5. Smeltzer, .E., Gulden, M.E., McElmury, S.S. and Compton, W.A., 1970, "Mechanisms of Sand and Dust Erosion in Gas Turbine Engines", USAAVLABS Technical Report 70-36.

6. Finnie, I., Wolak, J., and Kabin, C., 1967, "Erosion of Metals by Solid Particles", Jr. of Materials, 2, No. 3.

7. Winter, R.E. and Hutchings, I.M., 1975, "The Role of Adiabatic Shear in Solid Particle Erosion", Wear, 35, pp. 141-148.

8. Jennings, W.H., Manning, C.R., Jr., and Head, W.J., "A Mechanical Model for Prediction of Ductile Erosion", USAAMRDL-TR-75-30.

9. Hutchings, I.M., "Proceedings Corrosion/Erossion of Coal Conversion Materials Conference," N.A.C.E. (1979) p. 393.

10. Ruff, A.W. and Ives, L.K., 1975, "Measurement of Solid Particle Velocity in Erosive Wear", Wear, 35, pp. 169-182.

11. Rosenfield, A.L. and Hahn, G.T., Trans. Am. Soc. Metals, 59 (1966) p. 962.

12. Briggs, T.L. and Campbell, J.D., Acta Met., 20 (1972) p. 711.

13. Gulden, M.E., "Erosion Mechanisms of Metals," Second Annual Report, AFOSR Contract F49620-78-C-1040 (1980).

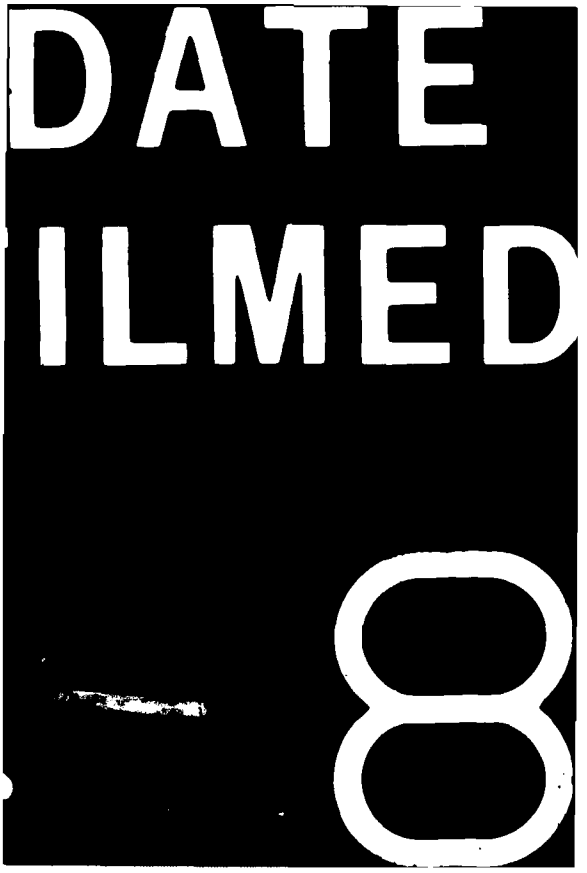
DATE
ILMED
8